Supporting Information

Tailored ternary hetero-interfaces with in-situ formed CNTs for effective electromagnetic coupling in low/mid-frequency

Jing Chen[1, a], Hong-Han Wang[1, a], Qing-Da An[a], Zuo-Yi Xiao[a], Xiao-Ling Dong[*,a], Kai-Ruo Zhu[a], Shang-Ru Zhai[*,a]

Liaoning Key Lab of Lignocellulose Chemistry and BioMaterials, Liaoning Collaborative Innovation Center for Lignocellulosic Biorefinery, College of Light Industry and Chemical Engineering, Dalian Polytechnic University, Dalian 116034, China

Corresponding authors:

E-mail: dongxiaoling@dlpu.edu.cn (X.L. Dong)

E-mail: zhaisr@dlpu.edu.cn (S.R. Zhai)

Materials

Cobalt nitrate hexahydrate ($Co(NO_3)_2 \cdot 6H_2O$, AR, 99%), manganese chloride tetrahydrate ($MnCl_2 \cdot 4H_2O$, AR, 99%), 2,5-dihydroxyterephthalic acid (H_4DOT, HPLC, ≥98.0%), and melamine (99%) were purchased from Aladdin. N, N-Dimethylformamide (DMF, AR) was purchased from Tianjin Komeo Chemical Reagent Co. Anhydrous ethanol (Ethanol, AR) was purchased from Tianjin Fuyu Fine Chemical Co.

Characterization

The microstructure, morphology, and elemental distribution of the samples were observed by field emission scanning electron microscopy (SEM, JSM-7800F), energy spectrometry (EDS), and transmission electron microscopy (TEM, JEOL-JEM 2100 F). The crystalline phases of the composites were analyzed using an x-ray diffractometer (XRD, 6100, SHIMADZU, Japan) with a radiation source of Cu Kα (40.0 kV, 30.0 mA), a scanning rate of 2 °/min, and a scanning range of 10.0 °~ 80.0 °. Raman spectra were obtained using a Raman microscope (Renishaw PLC) to analyze the composites' graphitization degree. N_2 adsorption-desorption measurements and specific surface areas of the samples were described using the Brunauer-Emmett-Teller (BET, JWBK222, China) method. The element composition and chemical bonding states of the samples were analyzed using X-ray photoelectron spectroscopy (XPS). EM parameters in the 2~18 GHz were performed using an Agilent E5071C Vector Network Analyzer (VNA) with the coaxial transmission line method. The samples containing 70wt% paraffin have pressed the mixture into a coaxial ring, the

inner diameter is 3.04 mm, the outer diameter is 7.00 mm. Based on the transmission line theory, the RL value of the sample was calculated using the S1.

Supplement to the main text

The relative complex permittivity ($\varepsilon_r = \varepsilon'-j\varepsilon''$) and relative complex permeability ($\mu_r = \mu'-j\mu''$) directly affect the EMW absorption performance. The real parts (ε' and μ') are typically used to assess the ability to store EM energy, and the imaginary parts (ε" and μ") are used to assess the ability to dissipate EM energy.

In general, the main sources of magnetic loss are eddy current loss and ferromagnetic resonance (natural resonance, exchange resonance).

S1. EM parameters and EMW absorption performance calculation

$$\varepsilon_r = \varepsilon' - j\varepsilon'' \tag{E1}$$

ε_r and μ_r represent the complex permittivity and permeability, ε' and ε" represent the real part of permittivity and imaginary part of permittivity.

$$\mu_r = \mu' - j\mu'' \tag{E2}$$

μ' and μ" represent the real part of permeability and imaginary part of permeability. Z_0 is the impedance of free space.

$$RL = 20log_{10} \left| (Z_{in} - Z_0) / (Z_{in} + Z_0) \right| \tag{E3}$$

Z_{in} is the input impedance of the absorber.

$$Z_{in} = Z_0 \sqrt{\mu_r / \varepsilon_r} tanh\left[j(2\pi fd) / c\sqrt{\mu_r \varepsilon_r} \right] \tag{E4}$$

f is the frequency of the EMW, d refers to the coating thickness of the absorber, and c represents the speed of light of the EMW in the free space.

$$Z = | Z_{in} / Z_0 | = | \sqrt{\mu_r / \varepsilon_r} tanh\left[2\pi jfd / c\sqrt{\mu_r \varepsilon_r} \right] | \quad \text{(E5)}$$

$$\alpha = \sqrt{2}\pi f / c\sqrt{\left(\mu''\varepsilon'' - \mu'\varepsilon'\right) + \sqrt{\left(\mu''\varepsilon'' - \mu'\varepsilon'\right)^2 + \left(\mu''\varepsilon' + \mu'\varepsilon''\right)^2}} \quad \text{(E6)}$$

$$\varepsilon'' = \left(\varepsilon_s - \varepsilon_\infty\right) \frac{2\pi f\tau}{1 + \left(2\pi f\right)^2 \tau^2} + \frac{\sigma}{2\pi f\varepsilon_0} \quad \text{(E7)}$$

where is the static permittivity, is the relative permittivity at the high-frequency limit, is the EMW frequency, is the polarization relaxation time and is the electrical conductivity, and is the dielectric constant of vacuum.

$$\left(\varepsilon' - \frac{\varepsilon_s + \varepsilon_\infty}{2} \right)^2 + \left(\varepsilon''\right)^2 = \left(\frac{\varepsilon_s - \varepsilon_\infty}{2} \right)^2 \quad \text{(E8)}$$

where ε_s and ε_∞ are the static and optimized dielectric constants, respectively.

$$\varepsilon' = \frac{1\varepsilon''}{2\pi f\tau} + \varepsilon_\infty \quad \text{(E9)}$$

$$C_0 = \mu''\left(\mu'\right)^{-2} f^{-1} = 2\pi\sigma d^2 \mu_0 \quad \text{(E10)}$$

S2. Figures

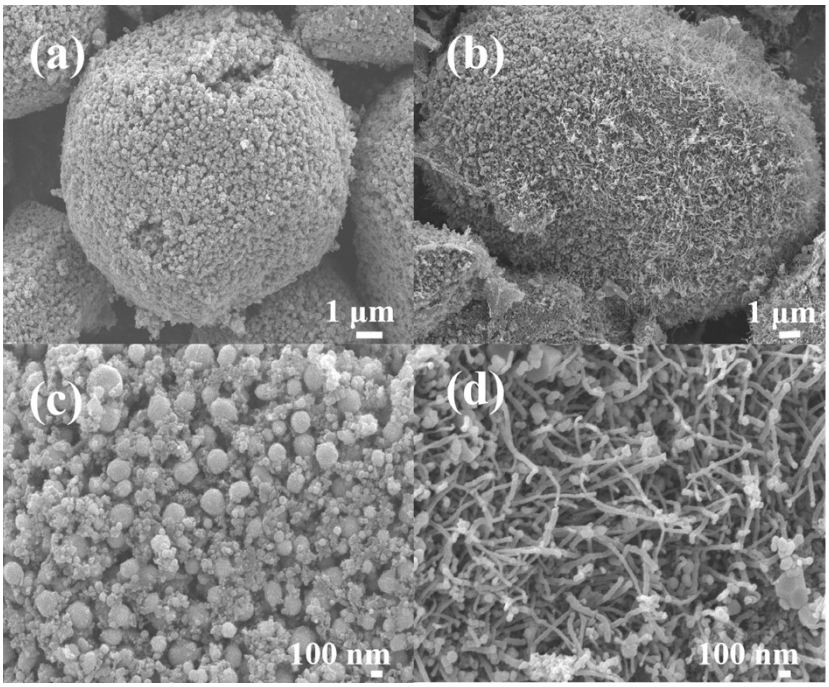

Fig. S1 SEM images of (a, c) Co/MnO@C and (b, d) Co/MnO@NC-6 with different dimensions.

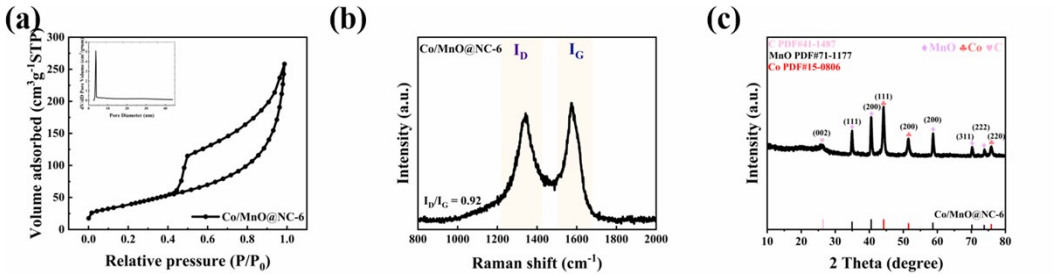

Fig. S2 (a) N_2 adsorption-desorption isotherms of Co/MnO@NC-6, (b) Raman spectra of Co/MnO@NC-6, (c) XRD pattern of Co/MnO@NC-6.

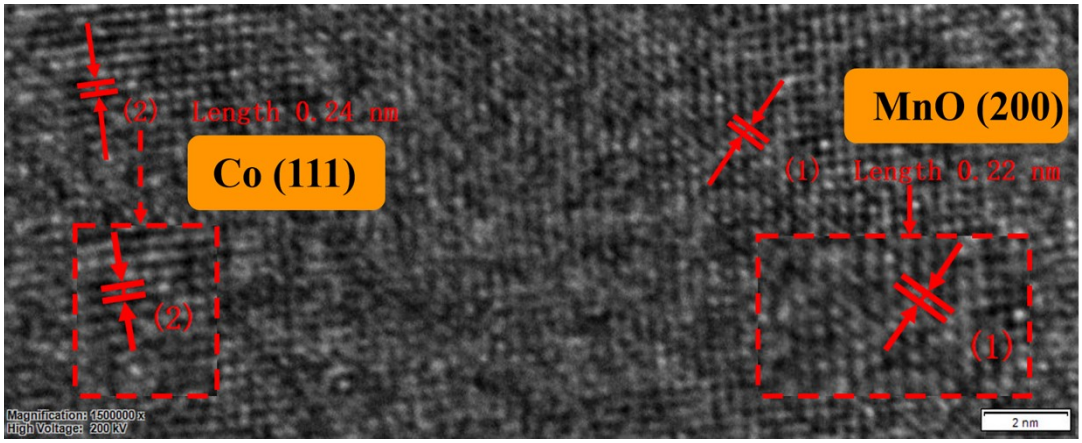

Fig. S3 Enlarged detail of lattice fringes of face-centered cubic Co and cubic MnO.

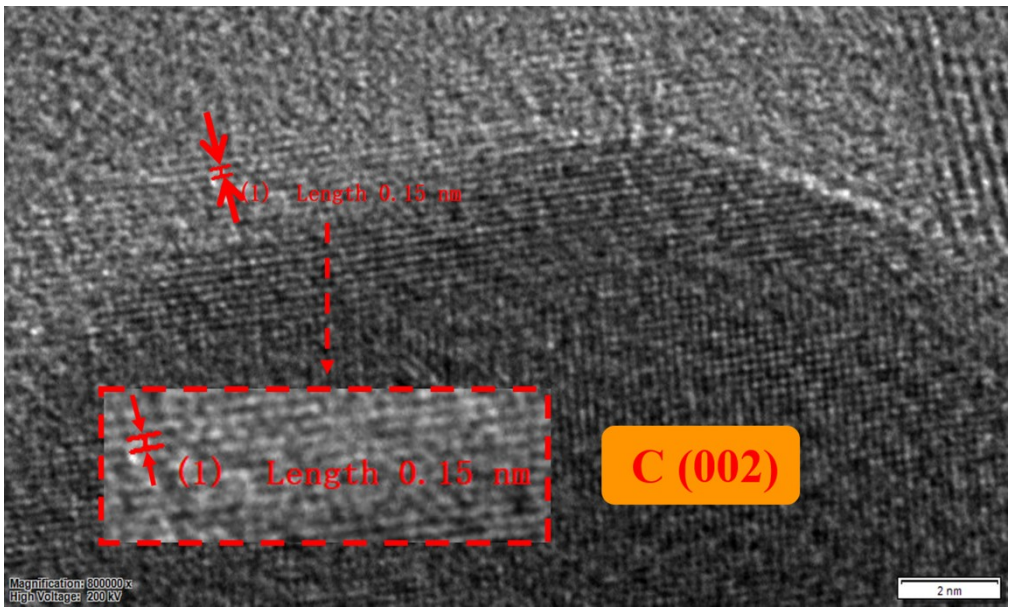

Fig. S4 The HRTEM image of graphite carbon.

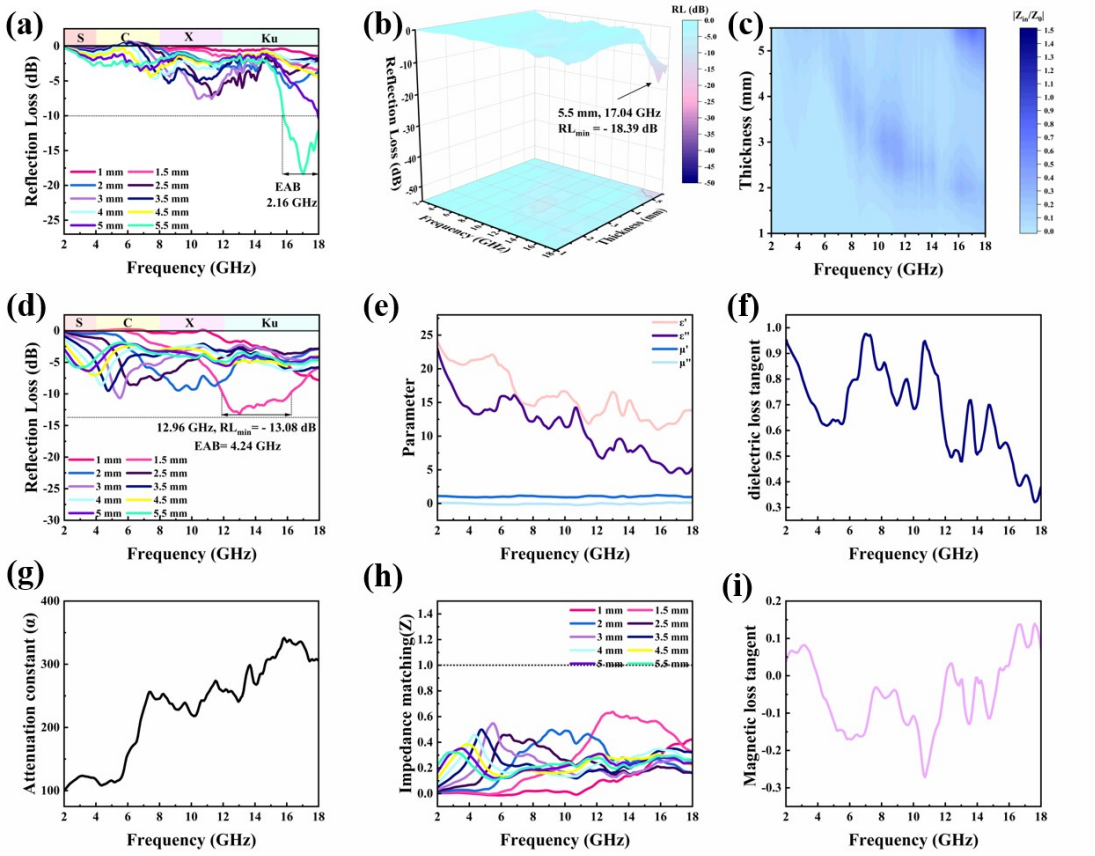

Fig. S5 (a) 2D images, (b) 3D images of calculated RL values and (c) 2D impedance matching contour maps of Co/MnO@NC-1, (d) RL plot, (e) EM parameter plot, (f) dielectric loss tangent plot, (g) α plot, (h) impedance matching plot, (i) magnetic loss tangent plot of Co/MnO@NC-6.

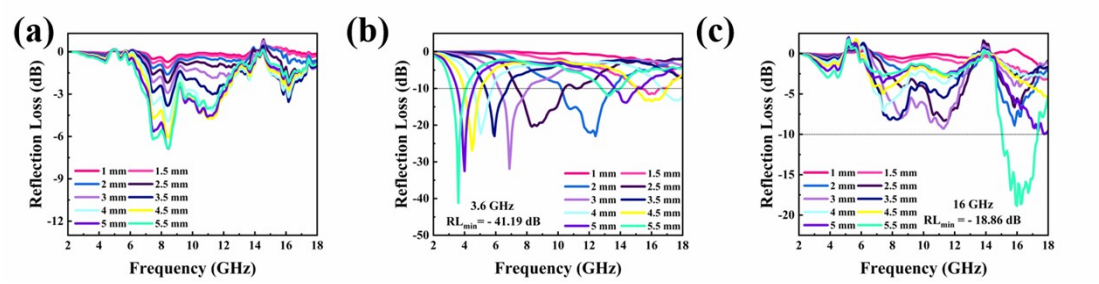

Fig. S6 Reflection loss of Co/MnO@NC-3 at different carbonization temperatures (a) 700 ℃ for 2h; (b) 800 ℃ for 2h; (d) 900 ℃ for 2h.

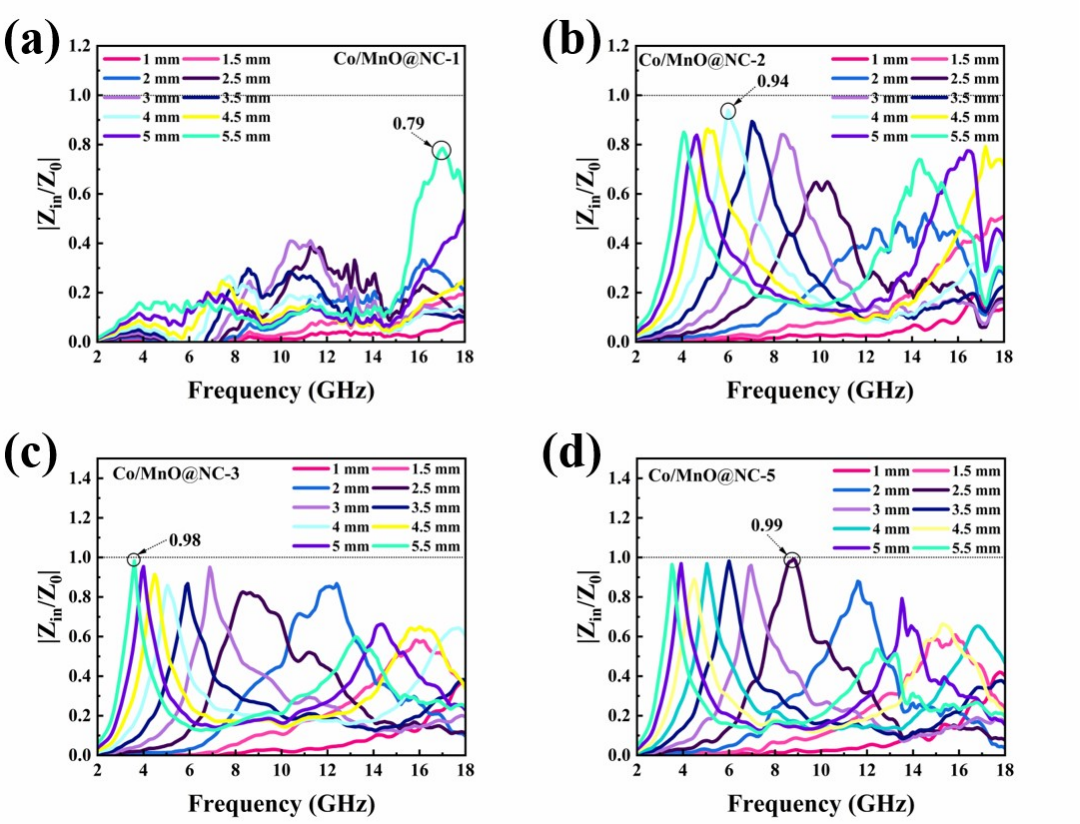

Fig. S7 Fine analysis of impedance matching plots for Co/MnO@NC-X (1, 2, 3, 5).

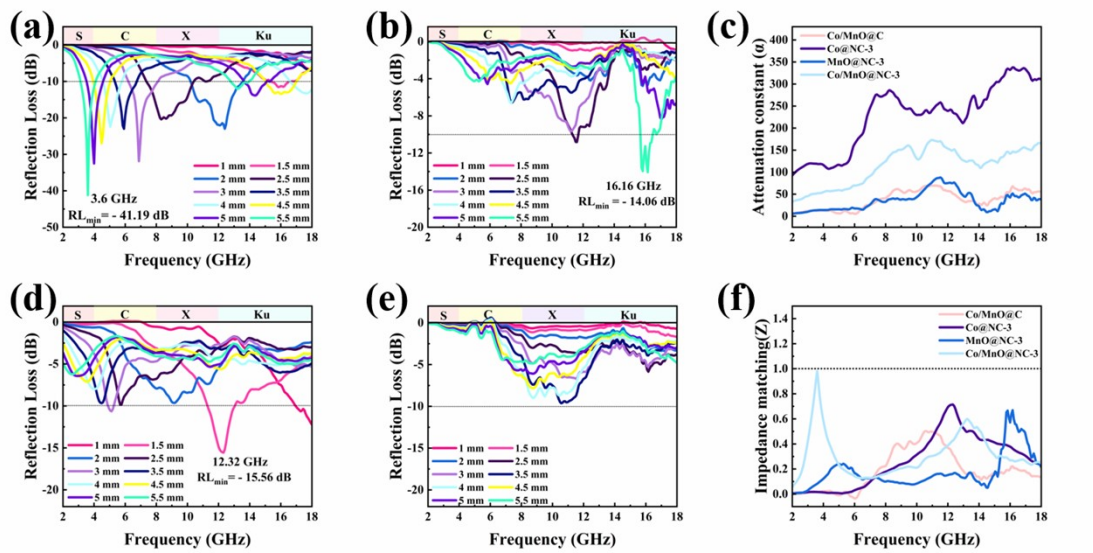

Fig. S8 RL plots of (a) Co/MnO@NC-3, (b) MnO@NC-3, (d) Co@NC-3, (e) Co/MnO@C; (c) α and (f) Z of comparison samples.

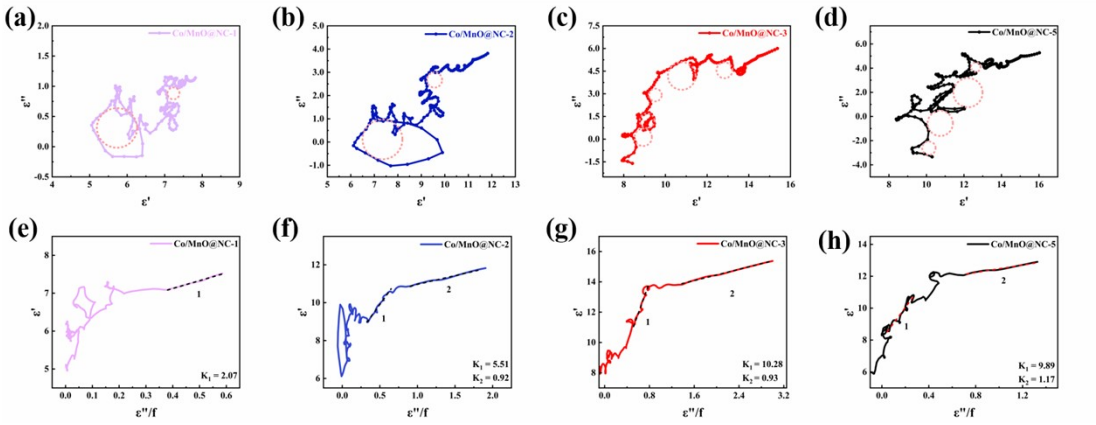

Fig. S9 The Cole-Cole plots of (a) Co/MnO@NC-1, (b) Co/MnO@NC-2, (c) Co/MnO@NC-3, (d) Co/MnO@NC-5, the relationship between ε' and ε''/f values of (e) Co/MnO@NC-1, (f) Co/MnO@NC-2, (g) Co/MnO@NC-3, (h) Co/MnO@NC-5.

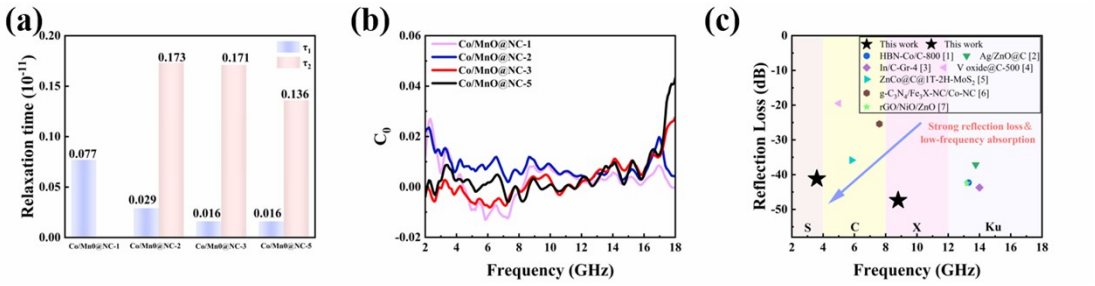

Fig. S10 (a) The relaxation time of Co/MnO@NC-X (X=1, 2, 3, 5), (b) C_0 of Co/MnO@NC-X (X=1, 2, 3, 5), (c) comparison of the EMW absorbing properties with other composites.